eurasia

Improving the Stability of Ink-Jet Printed Red QLEDs by Optimizing the Device Fabrication Process

**Halide Diker[a], Secil Sevim Unluturk[b],
Serdar Ozcelik[c], Canan Varlikli[d]**

Abstract: Red-light emitting Cadmium Sulfide$_{0.8}$ Selenide$_{0.2}$ / Zinc Sulfide ($CdS_{0.8}Se_{0.2}/ZnS$) based quantum dots (QDs) were synthesized by hot injection method and utilized as the emissive layer in the quantum dot light emitting diode (QLED) with the device structure of Indium Tin Oxide/Poly(3,4-ethylenedioxythiophene): Polystyrene Sulfonate /***Polyvinylcarbazole(or Poly (N,N'-bis-4-butylphenyl-N,N'-bisphenyl)benzidin)***/QD/ZincOxide/ LithiumFluoride/ Aluminum [*ITO/ PEDOT: PSS/**PVK(or p-TPD)**/ QD/ZnO/LiF/Al*]. QD inks were formulated and prepared in octane: decane; (1/1, v/v) solvent system and mixed with the non-ionic surfactant, TritonX-100, to make the QD inks inkjet printable. In addition to the inkjet printing technique, spin coating was also employed to form the QD emissive layer for comparing device performance. Compared to the p-TPD-based QLED device, the PVK-based device fabricated via spin coating exhibited ~6-fold higher performance in terms of luminance and efficiency values. In the case of using the ink-jet printer, ~2-fold higher maximum luminance value and slightly lower external quantum efficiency at the lower current density region were obtained in the p-TPD-based device. Furthermore, compared to the PVK layer, the p-TPD layer provided higher device stability regardless of the coating method at the higher current density regions. We suggest that the coating method applied and the choice of hole transport layer (HTL) materials may control the device parameters..

Keywords: Quantum Dots; Red Quantum Dot Light Emitting Diode (QLED); QD Ink Formulation; Inkjet Printing; Hole Transport Material.

[a] Department of Photonics, Izmir Institute of Technology, Izmir, Turkey.
Solar Energy Institute, Ege University, Izmir, Turkey.
Corresponding Author: halide.diker@ege.edu.tr

[b] Department of Photonics, Izmir Institute of Technology, Izmir, Turkey.
Kansai Altan Paint Industry and Trade Inc., Izmir, Turkey

[c] Department of Chemistry, Izmir Institute of Technology, Izmir, Turkey.

[d] Department of Photonics, Izmir Institute of Technology, Izmir, Turkey.

1. INTRODUCTION

Quantum dot light-emitting diodes (QLEDs) have gained significant attention in display technology due to the superior properties of quantum dots (QDs) such as high material stability, narrow emission bandwidth, adjustable emission wavelength, high color purity, and cost-effective solution-based processability (García de Arquer *et al.,* 2021; Liu *et al.,* 2017; Yang *et al.,* 2018). Although the spin-coating technique is the most used fabrication method for solution-based QLEDs, it limits the application of QDs to display manufacturing because it does not allow large-scale fabrication and the QD layers to create individual pixel-based patterns such as red/green/blue (RGB) in full-color QLED display designs. For this reason, alternative solution-processed techniques such as transfer printing, electro-hydrodynamic (EHD) jet printing, fog deposition, and inkjet printing techniques are used

to create QD patterns in pixel-based display applications (Cho *et al.,* 2015; Kim *et al.,* 2015; Kim *et al.,* 2011; Zhu *et al.,* 2008). Among these printing techniques the inkjet printing method has become prevalent in the last decade due to it providing some benefits such as i) allowing mask-free micro-patterning, ii) printing the pattern exactly on the specified area of the substrate, iii) enabling the digital control of ink droplets in defined volume, iv) compatible with Roll-to-Roll processes used in industrial production, and v) being cost and time-efficient (Peng *et al.,* 2017; Zhan *et al.,* 2022). However, when using this method in QLED applications, some drawbacks affecting the film morphology had to be overcome, such as coffee ring effects, Marangoni flow, pinholes, and substrate damage/erosion from the solvent used in the QD ink. These parameters have been important when considering interfacial interactions in multilayered films (Liu *et al.,* 2017). The QD ink formulation has been a critical issue in achieving high-performance inkjet-printed QLEDs. Several studies have been carried out to formulate the optimum QD ink using various solvent mixtures that have different vapor pressure to control the jettability of QD inks via inkjet printers, to avoid the coffee ring effects on the film surface, and so obtain uniform QD film morphology (Jia *et al.,* 2021; Jiang *et al.,* 2016; Li *et al.,* 2020; Yang *et al.,* 2020; Zhan *et al.,* 2022). Haverinen *et al.,* have increased the external quantum efficiency of the red light-emitting QLED device structured with ITO/PEDOT:PSS/poly-TPD/QDs/TPBi/LiF/Al from 0.19% to 0.23% by changing the rheology of the CdSe/ZnS QD solution through utilizing the toluene:dichlorobenzene binary solvent mixture (v:v;1:1) instead of using chlorobenzene alone. Nevertheless, poor device performance results were explained by the uncompleted energy transfer between the layers due to the pinhole and exciplex formation (Haverinen *et al.,* 2009; Lin *et al.,* 2010). The orthogonality of the solvents commonly used in the preparation of QD inks, such as heptane, octane, decane, etc., has avoided the intermixing or erosion problems of HTL. However, they need to be mixed with some aromatic solvents to make the QD ink suitable for inkjet printing by adjusting their boiling point and viscosity (Kim *et al.,* 2021). Liu *et al.,* reported that the presence of the high boiling point and relatively high viscosity CHB solvent in the decane: CHB solvent system used in the ink preparation allowed the regulation of the QD film morphology by causing the formation of an optimum contact angle on the

poly (N,N′-bis-4-butylphenyl-N,N′-bisphenyl) benzidin (p-TPD) substrate. They achieved 4.4 cd/A of maximum luminance efficiency at the luminance of 1974 cd/m^2 (Liu *et al.,* 2017). Additionally, the utilization of the crosslinked HTL materials in the device structure has also been another strategy to prevent HTL erosion caused by the solvent system of the QD ink, thereby improving the device performance (Jia *et al.,* 2021; Xie *et al.,* 2022; Xiong *et al.,* 2019; Yi & Su, 2023; Zhan *et al.,* 2022). Xiong *et al.,* investigated the solvent resistance of the different kinds of HTL materials such as poly (9-vinlycarbazole) (PVK), p-TPD and poly[(9,9'-dioctylfluorenyl-2,7- diyl)-co-(4,4'-(N-(4-sec-butyl)) diphenylamine)] (TFB). They reported PVK exhibited the best solvent resistance against cyclohexylbenzene (CHB): indane solvent system included in QD ink and accordingly led to the best device performance results with the external quantum efficiency (EQE) of 17%. (Xiong *et al.,* 2019). Therefore, in the fabrication of an inkjet-printed QLED device with high performance, the choice of solvents in the QD ink formulation and the HTL materials is of critical importance to control the interfacial interactions between the HTL and QD layers and thus uniform the film morphology.

In this study, alkane mixture such as octane: decane (1/1, v/v) having different boiling points were utilized as the solvent mixture system and it mixed with the nonionic surfactant of TritonX-100 instead of using an aromatic solvent to adjust the rheological properties of the QD ink for ink-jet printing. The amount of the TritonX-100 on the QLED performances was investigated. Crosslinked PVK and p-TPD were preferred as HTL materials to fabricate the QLED devices. In addition, spin-coated QD layer-based devices were built to compare the fabrication methods for device performances. It was determined that the coating method affected the device's performance according to the type of HTL layer being either PVK or p-TPD. Compared to the p-TPD-based QLED device, the PVK-based device exhibited ~6-fold higher performance in terms of luminance and efficiency values as fabricated via the spin coater. In the case of using the ink-jet printer, ~2-fold higher maximum luminance value and approximately the same external quantum efficiency at the lower current density region were obtained in the p-TPD-based device. Furthermore, compared to the PVK layer, the p-TPD layer provided higher device stability regardless of the coating method at the higher current density regions. Utilization of

TritonX-100 allowed for formulating QD ink without the aromatic solvents that have been commonly used in literature for the inkjet printing method and the improved QLED device stability was performed on the p-TPD layer by the optimized QD formulation, as well.

2. MATERIALS AND METHODS

2.1. Materials

For the synthesis of red $CdS_{0.8}Se_{0.2}$/ZnS QDs cadmium acetate (Cd(Ac)$_2$, 99.9%); zinc acetate (Zn(Ac)$_2$, 99.9%); oleic acid (OA, 90%); 1-octadecene (ODE, 90%); selenium powder (Se, 99.9%); sulfur powder (S, 99.9%); hexane and ethanol were purchased from Sigma-Aldrich. Zinc acetate dihydrate (Zn(CH$_3$COO)$_2$ 2H$_2$O) to synthesize ZnO nanoparticles as ETL layer, and trioctylphosphine (TOP, 90%).

15 Ω/sq) were purchased from Lumtec. Poly(3,4-ethylenedioxythiophene)-poly(styrenesulfonate) (PEDOT: PSS), (Al4083) that was used as hole injection layer (HIL) was purchased from Clevios. Both of the hole transport layer (HTL) materials; Poly(9-vinylcarbazole) (PVK) and Poly(N,N′-bis-4-butylphenyl-N,N′-bisphenyl)benzidin (p-TPD), cathode materials; Aluminium (Al) and Lithium Fluoride (LiF) and solvents; (n-Hexane, octane, decane, methanol, ethanol, chlorobenzene) were obtained from Sigma-Aldrich.

2.2. Characterizations

Cleaning of ITO substrates was processed by ISOLAB ultrasonic bath and CUTE FC-10046 O$_2$ plasma system. Absorbance, photoluminescence (PL) spectra, and time-correlated single photon counting (TCSPC) measurements were recorded using an Edinburgh FS5 spectrophotometer. Zeta potential measurement system (Malvern Zetasizer Nano ZS) was used for the particle size distribution of synthesized QDs. XRD measurements were done by Perkin Elmer X-ray diffraction. Ligands were detected by Fourier Transform Infrared Spectroscopy (FTIR) (Perkin Elmer). QD film thickness values and 3D optical images were determined by KlaTencor MicroXM-100 optical profilometer. X-ray photoelectron spectrophotometer, XPS (Thermo Scientific K-Alpha) was utilized to determine the valance band energy of QD. All solutions were coated on the substrate via Laurell WS-400B-6NPP LITE spin

coater under atmospheric conditions. Inkjet-printed QD layers were printed *using* Fujifilm Dimatix DMP-2850 inkjet printer. A thermal evaporator integrated into LC Technology Solutions Glove Box system was used during the evaporation of cathode materials. The current density-voltage characteristics and electroluminescence (EL) performances of the QLED devices were performed with a Keithley 2400 programmable power source and Hamamatsu C9920-12 system, respectively. All devices were characterized under inert conditions.

2.3. Synthesis of red $CdS_{0.8}Se_{0.2}$/ZnS quantum dot

Red-emitting $CdS_{0.8}Se_{0.2}$/ZnS nanocrystals were synthesized by the hot injection method (Lee *et al.*, 2015). For the formation of $CdS_{0.8}Se_{0.2}$ core, firstly 1.1 mmol Cd(Ac)$_2$ was stirred in 7 mL OA at 150 °C under the nitrogen atmosphere, and then 20 mL ODE was added. The reaction temperature was raised to 300 °C and stirred for 1 hour under refluxing. After the Cd-oleate complex formed and the reaction temperature stabilized, TOP-S-Se complex formed individually by the mixture of 0.3 mL of TOP with 0.03 mmol S and 0.27 mmol Se was quickly added to the reaction flask at 300 °C. After 90 s, the thiol ligand (dodecanethiol or octanethiol) was quickly added, and the reaction temperature was reduced to 270 °C. At this stage, the core structure, $CdS_{0.8}Se_{0.2}$ is formed. The zinc and sulfur sources for the shell structure were prepared by dissolving 2.86 mmol of Zn(Ac)$_2$ in 4 mL of OA and 1 mL of ODE. When the mixture was ready it was added dropwise to the reaction medium. Then the TOP-S complex formed with 6.35 mmol S and 3.5 mL TOP was added dropwise, too. After 10 minutes, the reaction medium was allowed to cool to room temperature, and the reaction was terminated. Nanocrystals were diluted with hexane and precipitated by adding ethanol. After 15 minutes of centrifugation at 6000 rpm, the precipitated solid nanoparticles were again dispersed in hexane and the purification process was repeated. If necessary, colloidal particles can be dispersed in organic solvents such as hexane, octane, and toluene or stored as solid.

2.4. Ligand Exchange Procedure

Dodecanethiol (DDT)-coated $CdS_{0.8}Se_{0.2}$/ZnS nanocrystals with a concentration of 20 mg/mL were prepared in 2.5 mL toluene and 35 µL

2-ethylhexanediol (EHT). The solution was stirred for 2 h at 70°C under refluxing and then the solution was precipitated by the addition of ethanol (1:1 by volume). After centrifugation at 6000 rpm for 15 min, the DDT ligands separated from the surface of the nanocrystals and unreacted free EHT ligands were removed. The solid QDs were dispersed again with 2 mL of toluene and the coating procedure was repeated with 20 µL of EHT. The reaction was stirred for 1 hour at the same reaction parameters. The EHT-coated $CdS_{0.8}Se_{0.2}$/ZnS nanocrystals were precipitated with ethanol and separated by centrifugation. The QDs can be stored in solid form or redispersed in toluene or another organic solvent like hexane, or octane for photophysical characterization.

2.5. Fabrication of inkjet-printed red QLEDs

7 mg/ml of QD solution in octane: decane solvent mixture (v:v;1:1) was mixed with *various* weight ratios (wt.%) of TritonX-100 (0.23%, 0.46%, 0.69% and 1.36%) to optimize the QD solution jettability. Hereafter, TritonX-100 was abbreviated as TX-100 in text.

Two different device structures were designed according to both included amount of TX-100 in QD inks and the used HTL materials in the device structure:

> i) *ITO/PEDOT:PSS/PVK/**QD-(TX-100,wt.%)**/ ZnO/LiF/Al*
>
> ii) *ITO/PEDOT:PSS/**PVK or p-TPD**/ QD-(TX-100,0.69%)/ZnO/LiF/Al*

Before QLED fabrication, 3D optical images and thickness values of the inkjet-printed QD films on the PVK layer were examined using an optical profilometer. This investigation aimed to establish the relationship between the thickness of the QD film and the performance of the QLED device, based on varying TX-100 weight ratios. (Table 1).

ITO substrates were etched and cleaned by a routine method (Diker *et al.*, 2020). Firstly, PEDOT: PSS was spin-coated on pre-patterned and pre-cleaned ITO substrates at 3000 rpm for 30 sec. and annealed at 120 °C for 20 min. PVK or p-TPD solution (10mg/mL, in chlorobenzene), which was utilized as a hole transport layer (HTL), was coated at 2000 rpm for 30 sec. on PEDOT: PSS layer and annealed at 150 °C for 10 min. Then QD inks

with different amounts of TX-100 were filtered by the 0.45µm pore-sized filter paper and then inkjet printed on the HTL layer separately and annealed at 160 °C for 30 min. Two-layer QD ink printing (layer by layer) was performed *while keeping other inkjet printer parameters fixed, i.e.; drop space: 45 µm, jetting voltage: 18V, substrate and ink temperatures: 25 °C.* Synthesized ZnO solution (10 mg/ml, in ethanol) according to a previous study (Ozguler *et al.*, 2020) which was used as an electron transport layer (ETL) was spin-coated on the QD emissive layer at 1500 rpm for 30 sec. and annealed at 160 °C for 30 min. Finally, LiF (7 nm) and Al (100 nm) cathode materials were deposited onto ETL by thermal evaporation (0.5 and 5 Å/sec, respectively). The QLED device's active area was 7.5 mm^2.

3. RESULTS AND DISCUSSIONS

3.1. Characterization of $CdS_{0.8}Se_{0.2}$/ZnS QDs

$CdS_{0.8}Se_{0.2}$/ZnS nanocrystals emit between 605 and 630 nm relating to the particle size and alloy composition (Lee *et al.*, 2015). The rate of the reactant addition, mole ratios, reactivities to each other, and the reaction temperature significantly affect the nucleation step of the core nanoparticles and the shell thickness. UV-Vis absorption and PL emission spectra of the synthesized red emitted nanoparticles are shown in Fig. 1a. The 10 nm Stokes shift is observed between the maximum absorbance wavelength ($\lambda_{abs.max}$:625 nm) and the maximum emission wavelength (λPL_{max}:635 nm) of $CdS_{0.8}Se_{0.2}$/ZnS nanoparticles. The full width at half maximum (FWHM) of the PL emission peak is approximately 30 nm. The *inserted photograph* in Fig. 1a shows *the fluorescent color* of nanoparticles under UV light. Well-defined absorption *and emission* spectra show that *spectrally pure and mono dispersed* QDs were obtained. The crystal lattices of the nanocrystals have a "zinc blende" structure according to the XRD diffractogram shown in Fig. 1b. Three specific diffraction peaks located at Bragg angles (2 Theta values) of 26.36°, 43.85° and 51.89° which are assigned to *hkl* planes of zinc blend crystal structure and indexed as (111), (220), and (311) planes, respectively. The existence of the observed diffraction peaks clearly without any impurities confirms the optical spectra as well. The diffraction patterns shown in orange, blue, and green indicate the 2 theta angles of the "zinc blende" crystal structures

of CdS, CdSe, and ZnS bulk structures, respectively. The diffractogram shows that nanocrystals have CdS rich structure with the alloy composition $CdS_{0.8}Se_{0.2}/ZnS$.

The addition of the thiol ligand after the formation of core $CdS_{0.8}Se_{0.2}$ nanocrystals was also investigated in terms of photophysical properties. An average lifetime because of three different photophysical processes was obtained by fitting the lifetime curves of four different samples. As shown in Fig. S1 and Table S1, the lifetimes, denoted as t_1, t_2, and t_3, are given as Rel%1, Rel%2, and Rel%3 for the percentage contributions of the processes mentioned. From Table S1, similar average lifetimes were obtained for the samples containing thiol ligands. It can be observed that there is a significant decrease *in the average lifetime* for

the sample without thiol ligand. These results *suggest* that the amount and the length of the alkyl chain do not affect the photophysical properties of the nanocrystals and that 1.7 mmol dodecanethiol ligand was used for the rest of the studies due to the relatively higher average lifetime values. Considering the effect of the ligand covered to the surface of core/shell nanocrystals on the device performance, it was demonstrated that ligands with highly-branched structures are preferred (Li *et al.,* 2019; Li *et al.,* 2019; Xie *et al.,* 2019). QDs having ligands with highly-branched structures can be prepared in a concentration of 1000-fold higher dispersibility (Yang *et al.,* 2016). For this purpose, the ligands on the surface nanocrystals (totally, TOP, and DDT) were changed with 2-ethylhexanthiol by ligand-exchange procedures.
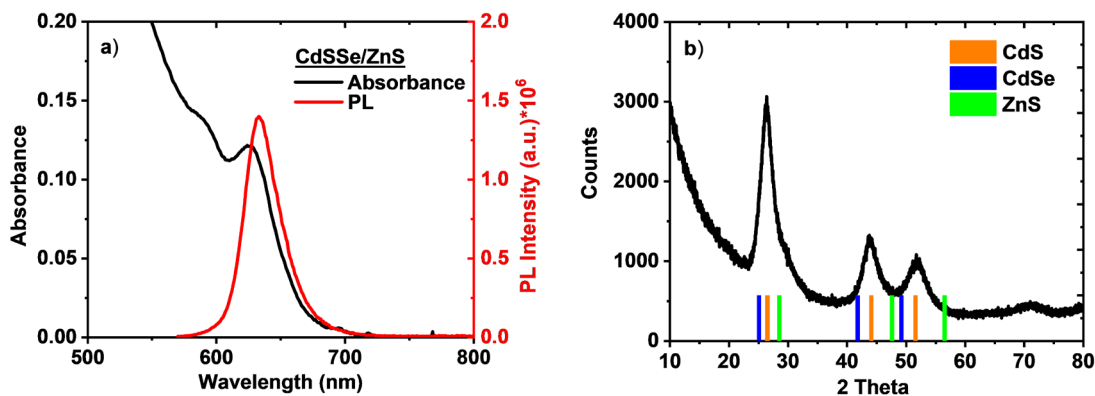

Figure 1. a) Absorbance and photoluminescence spectra and b) XRD spectrum of CdSSe/ZnS with the orange, blue and green diffraction patterns of bulk CdS, CdSe and ZnS structures, respectively. Well-defined absorption shoulder and low FWHM of PL peak confirm the high quality, purity, and monodispersity of the QDs.

Photophysical measurements of DDT- and EHT-coated QDs were performed and compared after ligand exchange procedures. The absorption and PL peak characteristics of the QDs, the absorption and emission spectra of which are shown in Fig. 2a, do not show any significant differences. *Due to the optical resolution (the slit width and the grating combined) of the spectrophotometer*, the shift towards the blue region of about 3 nm can be considered insignificant. On the other hand, the DLS measurements show that the particle sizes differ from each other (Fig. 2b). EHT-coated QDs have an average diameter of 5 nm. DDT-capped QDs have an average diameter of 8.5 nm. The ligand exchange procedure also improves the monodispersity of the nanoparticles. As DLS measures hydrodynamic diameter rather than nanoparticle core size, this difference is mainly due to the longer length

of DDT compared to EHT. The particle size of the core $CdS_{0.8}Se_{0.2}/ZnS$ does not change, only the shell thickness of the organic capping agent varies. Consequently, the particle size decreases while the optical spectra remain unchanged. The EHT-coated QDs obtained by ligand exchange have a longer lifetime as shown by the lifetime decay in Fig. 2c. The average lifetimes of the QD are 18.5 ns and 21.1 ns for DDT- and EHT-coated QDs, respectively.

Fig. 3a shows the FTIR spectra of DDT and EHT ligands and $CdS_{0.8}Se_{0.2}/ZnS$ particles to which these ligands are attached. The presence of most of the bands of DDT and EHT ligands in the spectra of QDs is an indication of a successful ligand exchange procedure. The spectra of DDT and EHT exhibit peaks at 2926 cm⁻¹ and 2854 cm⁻¹, which correspond to symmetric and asymmetric methylene stretching modes, respectively. Peaks between
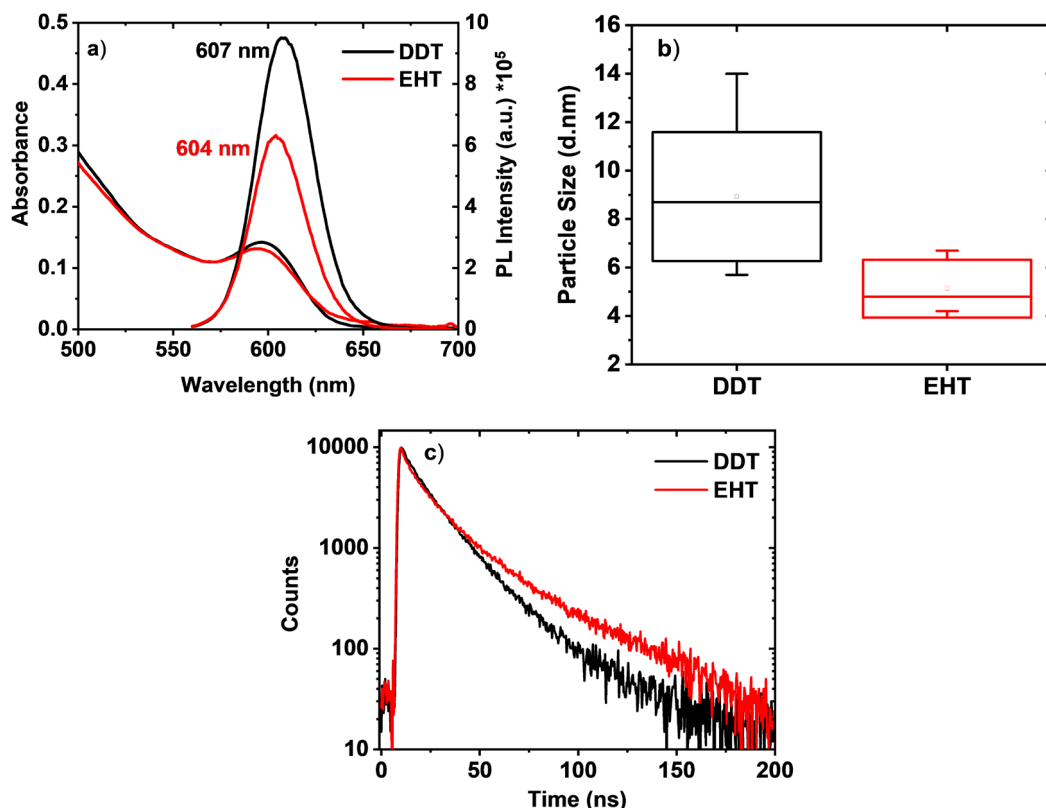
Figure 2. a) Absorption, photoluminescence spectra, and b) particle size distribution obtained from DLS and c) TCSPC measurements of DDT (before ligand exchange) and EHT coated (after ligand exchange) QDs.

1000 cm^{-1} and 1500 cm^{-1} are also observed, corresponding to C-H bending and fluctuation vibrations, as well as C-C stretching vibrations (Singh *et al.*, 2020). The spectra of DDT- and EHT-coated QDs show similar peaks. The peaks at 655 and 666 cm^{-1} in the spectra of pure DDT and EHT, respectively, correspond to the C-S stretching vibration of the thiol ligand. The peaks at 2565 cm^{-1} and 2570 cm^{-1} are attributed to the S-H stretching vibration. Thiol surfactant ligands are predicted to bind to QD surfaces through the sulfur. The absence of peaks belonging to C-S and S-H bonds in pure DDT and EHT ligands in the FTIR spectra of QDs supports this prediction (refer to Figs. 3b and c) (Pal & Kryschi, 2015). The EHT and DDT bands, which are structurally similar in terms of functional groups, produce similar peaks in the FTIR spectrum. In ligand-coated QDs, the C-H and C-C stretching vibrations are not prominent in the spectra due to low signal. Nevertheless, the C-S band around 650 cm^{-1} shifts towards a higher wave number in DDT and EHT-bonded QDs. This shift occurs because the sulfur bonding with the metal is stronger in the C-S bond than in the free state (Li *et al.*, 2016).

The band gap of the nanoparticles was calculated from XPS and absorption spectra. The valence band energy level of the dodecanethiol caped CdS$_{0.8}$Se$_{0.2}$/ZnS nanoparticles was obtained from the XPS valence spectrum (Fig. 4) as mentioned in our previous study (Ozguler *et al.*, 2020). The valence band was calculated as -5.4 eV and the addition of the optical band gap obtained from absorption spectra (2.1 eV) gives the -3.3 eV as the conduction band energy level.

3.2. Inkjet-Printed CdS$_{0.8}$Se$_{0.2}$/ZnS QD Films and Fabrication of QLED devices

Before forming the inkjet-printed QD films and QLED devices, spin-coated QD thin films and corresponding QLED devices were fabricated with two kinds of QD solution concentrations, i.e., 1 mg/mL and 7 mg/mL, to optimize the performance of the spin-coated device. The 3D optical profilometer images, thickness values, and photophysical characterization results of these QD thin films are given in Table S2 and Fig. S2. The electroluminescent properties of these QD films were investigated
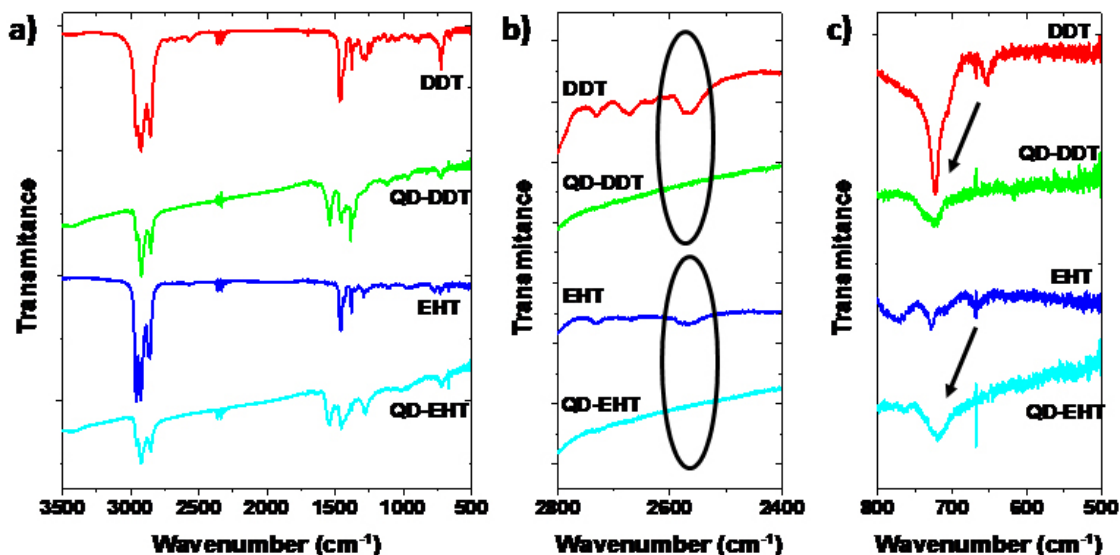
Figure 3. a) Full FTIR spectra of DDT- and EHT-coated $CdS_{0.8}Se_{0.2}$/ZnS structures with free EHT and DDT ligands, b) FTIR spectra in the range of 2800 to 2400 cm^{-1} showing the S-H bond bands and c) the range of 500 to 800 cm^{-1} showing the C-S bond bands.
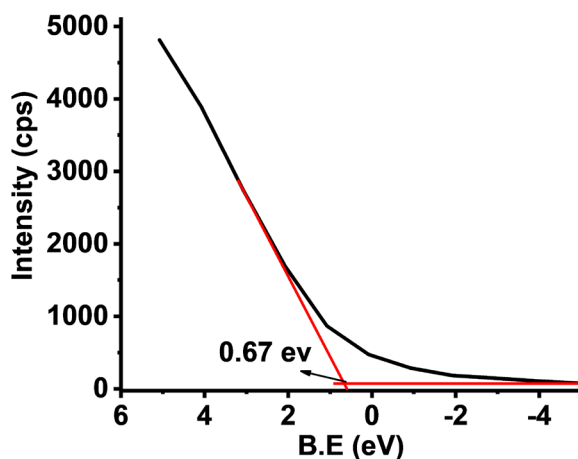

Figure 4. XPS valence spectrum of dodecanethiol capped $CdS_{0.8}Se_{0.2}$/ZnS nanoparticles. Red lines show the onset of the valence band obtained as 0.67 eV.

through the QLED with the device architecture i.e.; *"ITO/PEDOT: PSS/p-TPD/QD(d,x)/ZnO/LiF/Al"*. QD(d,x) represents the QD film thickness values based on the solution concentration and multilayer coating process. The effect of the QD film thickness on the device performance results is discussed in the Supporting Information (SI). While the optimum luminance and efficiency values were obtained for the device fabricated via 7mg/ml QD solution concentration (form 30 nm-thick QD layer) (Fig. S3), this concentration was utilized to prepare inkjet-printed QD layers and QLED devices.

Four different QD inks were prepared by adding four different amounts of TX-100 surfactant (0.23%, 0.46%, 0.69%, and 1.36% by weight) *to* the QD solution prepared in octane: decane (1:1, v/v) solvent system. These QD inks were used as inkjet printed emissive layers in the QLEDs with the device architecture of *"ITO/PEDOT:PSS/PVK/QD-(TX-100,wt.%)/ZnO/LiF/Al"* to investigate the effect of the TX-100 on the device performance results (Fig. S4). The maximum luminance voltage values did not change depending on the amount of TX-100 (except for TX-100; 1.36%) and the working voltage

($V_{turn-on}$) values obtained for all samples were in the range of 6-7 V. The highest luminance value (110.20 cd/m^2) was obtained for the TX-100; 0.69% based device due to owing the ~1.5 times thicker QD layer (25.1 ± 7.5 nm thickness) compared to the TX-100; 0.21% and 0.43% based ones (Table 1). It is thought that the lower amount of TX-100, in the case of 0.21% and 0.43%, may cause the QD ink to spread over the larger substrate area, forming a thinner film and therefore reducing the luminance due to the decreased amount of QD per unit area. On the other hand, the excess amount of TX-100 (1.36 %) was thought to act as an insulator material in the system and thus reduced the radiative recombination possibility through decreased charge mobility. Additionally, the shifts in the maximum EL wavelength ($\Delta\lambda_{ELmax.}$) depending on the applied voltage were negligible (5-6 nm) and the obtained light was in the red region of the color coordinate diagram [(x,y) (~0.60,0.31)] for all devices (Fig. S5). The optimum device performance results were obtained for the TX-100; 0.69 % included ink-based devices. Also, that ink was utilized for further inkjet printed device fabrication with the architecture of *"ITO/ PEDOT: PSS/**PVK or p-TPD**/QD-(TX-100,0.69%)/ ZnO/LiF/Al"* to investigate the effect of the HTL layer materials on the device performances. In addition, the performance results of devices containing spin-coated QD layers were compared with those of inkjet-printed devices (Fig. 5). Dramatic differences in device performance results were observed with changing the HTL layer and coating method as well. The most distinctive difference with the use of p-TPD material instead of the PVK material was the significant decrement in $V_{turn-on}$ values of the devices, regardless of the differences in coating technique. This can be attributed to the disappearance of the energy barrier at the PEDOT: PSS/p-TPD interface, which is relatively high at the PEDOT: PSS/PVK interface (Fig. 6). In addition, since the HOMO energy level of the p-TPD (-5.2 eV) and the valence band energy level of the QD (-5.4 eV) were more compatible compared to that of the PVK (-5.8 eV) and therefore hole transfer from the p-TPD to the QD layer became easier and the possibility of radiative recombination in the emission layer increased. For this reason, the maximum luminance value obtained from the p-TPD-based device for inkjet-printed devices was slightly higher than that of the PVK-based device. In contrast, for the spin-coated devices, the maximum luminance value of the PVK-based device (152.78 cd/m^2) was ~6-fold

higher than that of the p-TPD-based one (25.01 cd/m^2). These unexpected results could be attributed to the utilization of the same annealing temperature (160 °C) for the PVK and p-TPD layers, and therefore the variation in the interactions between the QD/PVK and QD/p-TPD interfaces. Liu *et al.*, identified that the high annealing temperature of the p-TPD caused the formation of more durable films based on the successful crosslinking between the polymer backbone, thus inhibiting the erosion problem of the p-TPD film against the solvents of the upper layer material (Liu *et al.*, 2017). So, an insufficient annealing temperature may have resulted in the removal of some part of the p-TPD layer during the spin coating of the QD ink due to its solvent erosion effect and led to the formation of interfacial traps which resulted in non-radiative recombination during the EL processes (Gupta *et al.*, 2014; Ozguler *et al.*, 2020). However, in inkjet-printed devices, the erosion effect could lead to the intermixing of the p-TPD layer with the QD layer on the film and stimulate the balance charge injection. Therefore, it is thought that according to the HTL materials, different interfacial interactions occurred between the QD and HTL layers based on the coating techniques, and the type of HTL materials require different optimum annealing temperatures to achieve high device performances. It is observed that regardless of the differences in coating techniques, the EQE values of the PVK-based devices were higher than those of the p-TPD-based one in the low current density region, whereas they had low device stability at the high current density region. This could be explained by the extra charging of the QD layer due to the unbalanced charge carrier injection that resulted in Auger recombination (Ozguler *et al.*, 2020). On the contrary, the obtained higher stability in the p-TPD-based devices at high current density region, especially for the inkjet printing method, could be explained by the intermixing effect between the p-TPD and QD layers based on the HTL erosion. Contrary to the literature, this erosion phenomenon was considered to be beneficial, increasing the charge transport kinetics and suppressing the excess Joule heating due to the leakage current with increasing current density (Sun *et al.*, 2019). Regardless of the coating technique and HTL differences, the color of the radiation obtained for all devices was located in the red region in the color coordinate diagram (x,y; ~ 0.61, 0.32). Furthermore, the change in color coordinates depending on the applied voltage was negligible.

Amount of TritonX-100 (w,%)

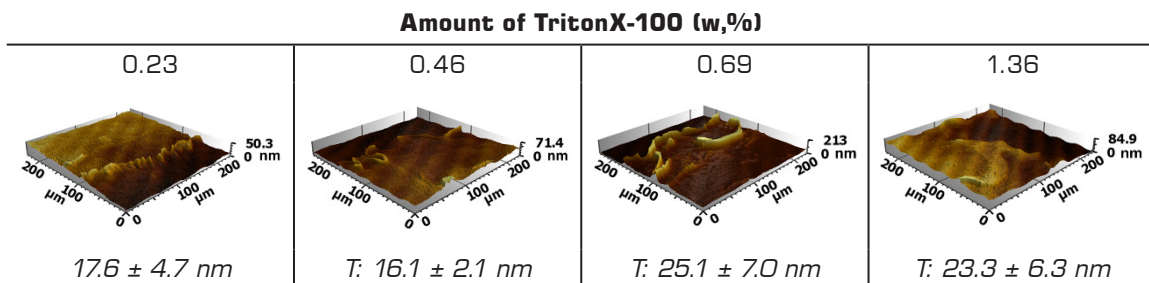| 0.23	0.46	0.69	1.36
17.6 ± 4.7 nm	T: 16.1 ± 2.1 nm	T: 25.1 ± 7.0 nm	T: 23.3 ± 6.3 nm

Table 1. 3D optical profilometer images and thickness values of inkjet printed QD layer on PVK layer based on included different amounts of TritonX-100 surfactant.
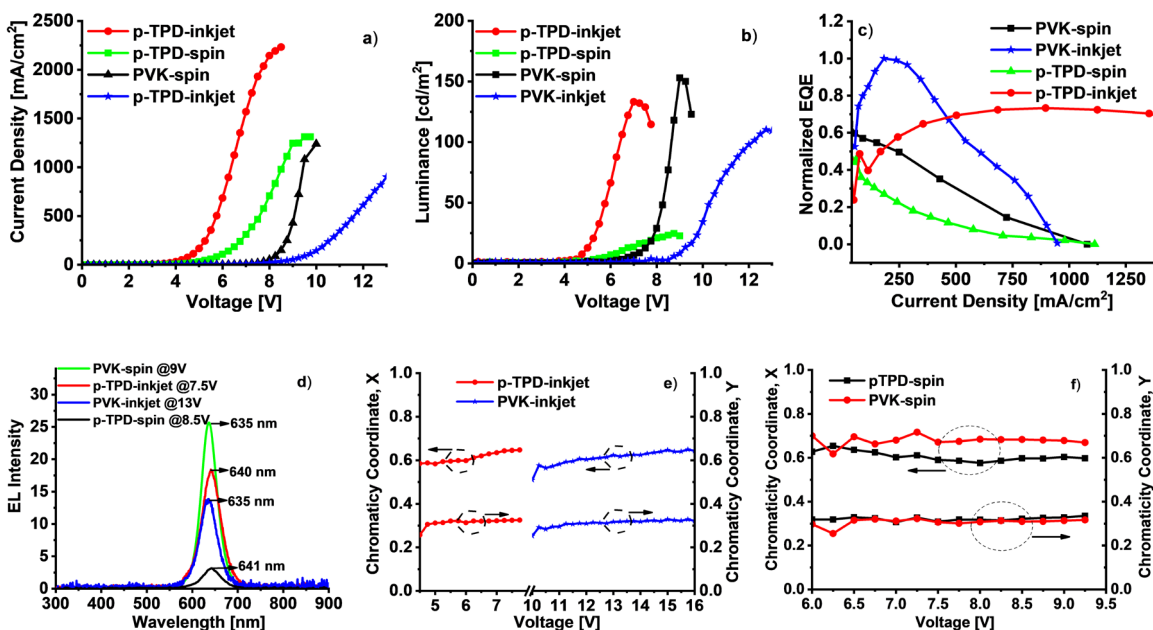

Figure 5. *Device* performances of inkjet-printed and spin-coated QLEDs with ITO/PEDOT: PSS/ PVK or p-TPD/QD/ZnO/LiF/Al device structure a) Current density-voltage curves, b) luminance-voltage curves, c) EQE- current density curves, d) EL- wavelength curves, e) X-color coordinate-voltage curves, f) X-color coordinate- voltage curves
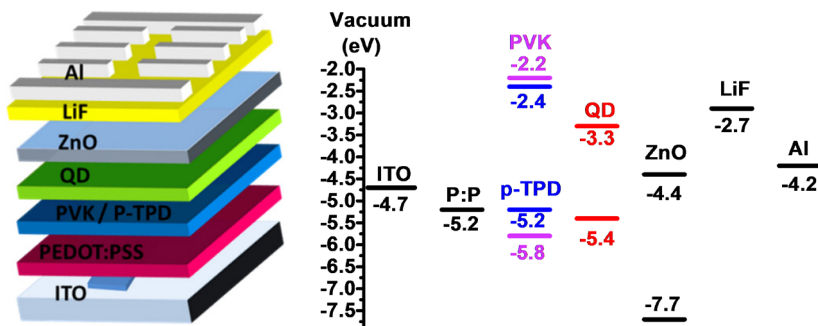

Figure 6. Cross-sectional image of QLED device and its energy level diagram [The valence band energy level and the conduction band energy level of QD were calculated through XPS valence band analysis and the optical energy band gap value determination from the absorption curve, respectively.].

4. CONCLUSION

Inkjet-printed red emitting QLEDs were fabricated by using ternary core-shell $CdS_{0.8}Se_{0.2}$/ZnS colloidal quantum dots. TritonX-100, a non-ionic surfactant, was mixed with the QD solution in an octane: decane; (1/1, v/v) solvent *mixture* to modulate the rheological properties of the QD ink for inkjet printing method. A systematic investigation into the influence of varying Triton X-100 amounts on QLED performance was conducted. The optimum TritonX-100 amount was determined as 0.69 % to achieve high device performance. The lower amount of TX-100, in the case of 0.21% and 0.43%, might cause the QD ink to spread over the larger substrate area, forming a thinner film and therefore reducing luminance due to the decreased amount of QD per unit area. Conversely, the excess amount of TX-100 (1.36 %) was thought to act as an insulator material in the system and thus reduced the radiative recombination possibility by decreasing the charge mobility. In addition, two types of HTL materials *i.e., PVK and p-TPD*, were also performed in the QLED fabrication process. It was determined that the coating method affected the device performance depending on the type of HTL materials such as PVK or p-TPD. It was thought that erosion of the p-TPD occurred due to the insufficient annealing temperature of the p-TPD layer, resulting in ~6-fold lower luminance value in the spin-coated QLED devices compared to the PVK-based one. However, this erosion effect caused intermixing of the p-TPD layer with the QD layer during the inkjet printing process, stimulated the balanced charge injection in the device structure, and thus resulted in 2-fold higher luminance values than PVK. Therefore, it is thought that according to the HTL materials, different interactions occurred at the interface between the QD and HTL layers based on the coating techniques, and the kind of HTL materials require different optimum annealing temperatures to achieve higher device performances. Although the p-TPD-based devices exhibited lower external quantum efficiency than the PVK-based devices regardless of the coating method, their higher stability at higher current density regions could be attributed to the increasing charge transport kinetics and the inhibition of the excess Joule heating probability.

Author Contributions

H.D.: Methodology, validation, formal analysis, and writing of the original draft. S.S.U.: Methodology, validation, formal analysis, and writing of the original draft. S.O.: Conceptualization, supervision, writing, reviewing, and editing and project administration. C.V.: Conceptualization, writing, review, editing, supervision, and project administration. All authors have read and agreed to the published version of the manuscript.

Acknowledgments

Conflict of Interest

The authors declare no competing financial interest. ♦

Abbreviation

QD	Quantum dot	Cd	Cadmium
QLED	Quantum dot light-emitting diode	Se	Selenium
HTL	Hole Transport Layer	S	Sulfur
ETL	Electron Transport Layer	CdS	Cadmium Sulfide
HIL	Hole Injection Layer	CdSe	Cadmium Selenide
ITO	Indium Tin Oxide	ZnS	Zinc Sulfide
PEDOT:PSS	Poly(3,4-ethylenedioxythiophene): Polystyrene Sulfonate	CdSSe	Cadmium Sulfide Selenide
PVK	Polyvinylcarbazole	DDT	Dodecanethiol
P-TPD	Poly(N,N′-bis-4-butylphenyl-N,N′-bisphenyl)benzidin	EHT	2-ethylhexanediol
TFB	Poly[(9,9'-dioctylfluorenyl-2,7-diyl)-co-(4,4'-(N-(4-sec-butyl)) diphenylamine)	$Cd(Ac)_2$	Cadmium Acetate
ZnO	Zinc Oxide	$Zn(Ac)_2$	Zinc Acetate

LiF	Lithium Fluoride	OA	Oleic Zcid
Al	Aluminum	ODE	1-octadecene
TX-100	TritonX-100	$Zn(CH_3COO)_2.2H_2O$	Zinc Acetate Dihydrate
(TCSPC)	Time-Correlated Single Photon Counting	TOP	Trioctylphosphine
XRD	X-Ray Diffraction	CHB	Cyclohexylbenzene
XPS	X-Ray Photoelectron Spectrophotometer	HOMO	Highest Occupied Molecular Orbital
FTIR	Fourier Transform Infrared Spectroscopy	$\lambda_{abs.max}$	Maximum Absorbance Wavelength
DLS	Dynamic Light Scattering	λ_{PLmax}	Maximum Emission Wavelength
PL	Photoluminescence	EQE	External Quantum Efficiency
EL	Electroluminescence	$V_{turn-on}$	Working Voltage

REFERENCES

Cho, H., Kwak, J., Lim, J., Park, M., Lee, D., Bae, W. K., Kim, Y. S., Char, K., Lee, S., & Lee, C. (2015). Soft Contact Transplanted Nanocrystal Quantum Dots for Light- Emitting Diodes: Effect of Surface Energy on Device Performance. *ACS Applied Materials and Interfaces, 7,* 10828-10833. https://doi.org/10.1021/acsami.5b01738

Diker, H., Bozkurt, H., & Varlikli, C. (2020). Dispersion stability of amine modified graphene oxides and their utilization in solution processed blue OLED. *Chemical Engineering Journal, 381,* 122716. https://doi.org/10.1016/j.cej.2019.122716

García de Arquer, F. P., Talapin, D. V., Klimov, V. I., Arakawa, Y., Bayer, M., & Sargent, E. H. (2021). Semiconductor quantum dots: Technological progress and future challenges. *Science, 373*(6555), eaaz8541. https://doi.org/10.1126/science.aaz8541

Gupta, S. K., Shankar, B., Taube, W. R., Singh, J., & Akhtar, J. (2014). Capacitance-conductance spectroscopic investigation of interfacial oxide layer in Ni/4H-SiC (0 0 0 1) Schottky diode. *Physica B: Condensed Matter, 434*(1), 44-50. https://doi.org/10.1016/j.physb.2013.10.042

Haverinen, H. M., Myllylä, R. A., & Jabbour, G. E. (2009). Inkjet printing of light emitting quantum dots. *Applied Physics Letters, 94*(7), 073108. https://doi.org/10.1063/1.3085771

Jia, S., Tang, H., Ma, J., Ding, S., Qu, X., Xu, B., Wu, Z., Li, G., Liu, P., Wang, K., & Sun, X. W. (2021). High Performance Inkjet-Printed Quantum-Dot Light-Emitting Diodes with High Operational Stability. *Advanced Optical Materials, 9*(22), 1-10. https://doi.org/10.1002/adom.202101069

Jiang, C., Zhong, Z., Liu, B., He, Z., Zou, J., Wang, L., Wang, J., Peng, J., & Cao, Y. (2016). Coffee-Ring-Free Quantum Dot Thin Film Using Inkjet Printing from a Mixed-Solvent System on Modified ZnO Transport Layer for Light- Emitting Devices. *ACS Applied Materials and Interfaces, 8,* 26162-26168. https://doi.org/10.1021/acsami.6b08679

Kim, B. H., Onses, M. S., Lim, J. Bin, Nam, S., Oh, N., Kim, H., Yu, K. J., Lee, J. W., Kim, J.-H., Kang, S.-K., Lee, C. H., Lee, J., Shin, J. H., Kim, N. H., Cecilia Leal, Shim, M., & Rogers, J. A. (2015). High-Resolution Patterns of Quantum Dots Formed by Electrohydrodynamic Jet Printing for Light-Emitting Diodes. *Nano Letters, 15,* 969-973. https://doi.org/10.1021/nl503779e

Kim, J. H., Kang, Y. J., & Chin, B. D. (2021). Solvent mixture formulation for orthogonal inkjet processing and uniform pixel patterning of quantum dot light-emitting diode. *Journal of the Korean Physical Society, 78*(11), 1116-1127. https://doi.org/10.1007/s40042-021-00153-8

Kim, T.-H., Cho, K.-S., Lee, E. K., Lee, S. J., Chae, J., Kim, J., Kim, D. H., Kwon, J.-Y., Amaratunga, G., Lee, S. Y., Choi, B. L., Kuk, Y., Kim, J. M., Kim, K., & Light-emitting. (2011). Full-colour quantum dot displays fabricated by transfer printing. *Nature Photonics, 5,* 176-182. https://doi.org/10.1038/nphoton.2011.12

Lee, K. H., Han, C. Y., Kang, H. D., Ko, H., Lee, C., Lee, J., Myoung, N. S., Yim, S. Y., & Yang, H. (2015). Highly Efficient, Color-Reproducible Full-Color Electroluminescent Devices Based on Red/Green/Blue Quantum Dot-Mixed Multilayer. *ACS Nano, 9*(11), 10941-10949. https://doi.org/10.1021/acsnano.5b05513

Li, G., Huang, J., Li, Y., Tang, J., & Jiang, Y. (2019). Highly bright and low turn-on voltage CsPbBr3 quantum dot LEDs via conjugation molecular ligand exchange. *Nano Research, 12*(1), 109-114. https://doi.org/10.1007/s12274-018-2187-5

Li, H., Duan, Y., Shao, Z., Zhang, G., Li, H., Huang, Y. A., & Yin, Z. (2020). High-Resolution Pixelated Light Emitting Diodes Based on Electrohydrodynamic Printing and Coffee-Ring-Free Quantum Dot Film. *Advanced Materials Technologies, 5*(10), 1-6. https://doi.org/10.1002/admt.202000401

Li, J., Jin, H., Wang, K., Xie, D., Xu, D., Xu, X., & Xu, G. (2016). High luminance of CuInS2-based yellow quantum dot light emitting diodes fabricated by all-solution processing. *RSC Advances, 6*(76), 72462-72470. https://doi.org/10.1039/c6ra14241a

Li, Y. F., Feng, J., & Sun, H. B. (2019). Perovskite quantum dots for light-emitting devices. *Nanoscale, 11*(41), 19119-19139. https://doi.org/10.1039/c9nr06191f

Lin, C., Hung, C., Kuo, P., & Cheng, M. (2010). Display Technology Letters. *Journal of Display Technology, 8*(12), 681-683. https://doi.org/10.1109/JDT.2009.2039019

Liu, Y., Li, F., Xu, Z., Zheng, C., Guo, T., Xie, X., Qian, L., Fu, D., & Yan, X. (2017). Efficient All-Solution Processed Quantum Dot Light Emitting Diodes Based on Inkjet Printing Technique. *ACS Applied Materials and Interfaces, 9,* 25506-25512. https://doi.org/10.1021/acsami.7b05381

Ozguler, S., Diker, H., Unluturk, S. S., Ozcelik, S., & Varlikli, C. (2020). Reducing the Efficiency Roll Off and Applied Potential-Induced Color Shifts in CdSe@ZnS/ZnS-Based Light-Emitting Diodes. *The Journal of Physical Chemistry C, 124,* 14847-14854. https://doi.org/10.1021/acs.jpcc.0c02769

Pal, N. K., & Kryschi, C. (2015). A facile one-pot synthesis of blue and red luminescent thiol stabilized gold nanoclusters: A thorough optical and microscopy study. *Physical Chemistry Chemical Physics, 17*(33), 21423-21431. https://doi.org/10.1039/c5cp01773d

Peng, X., Yuan, J., Shen, S., Gao, M., Chesman, A. S. R., Yin, H., Cheng, J., Zhang, Q., & Angmo, D. (2017). Perovskite and Organic Solar Cells Fabricated by Inkjet Printing: Progress and Prospects. *Advanced Functional Materials, 27*(41), 1703704. https://doi.org/10.1002/adfm.201703704

Singh, K., Kumar, A., Pandey, S. K., Awasthi, S., Gupta, S. P. & Mishra, P. (2020). Interpretation of Adsorption Behavior of Carboxymethyl Cellulose onto Functionalized Accurel Polymeric Surface. *Industrial & Engineering Chemistry Research, 59*(43),19102-19116. https://doi.org/10.1021/acs.iecr.0c03894

Sun, Y., Su, Q., Zhang, H., Wang, F., Zhang, S., & Chen, S. (2019). Investigation on Thermally Induced Efficiency Roll-Off: Toward Efficient and Ultrabright Quantum-Dot Light-Emitting Diodes. *ACS Nano, 13,* 11433-11442. https://doi.org/10.1021/acsnano.9b04879

Xie, L., Yang, J., Zhao, W., Yi, Y. Q. Q., Liu, Y., Su, W., Li, Q., Lei, W., & Cui, Z. (2022). High-Performance Inkjet-Printed Blue QLED Enabled by Crosslinked and Intertwined Hole Transport Layer. *Advanced Optical Materials, 10*(21), 1-9. https://doi.org/10.1002/adom.202200935

Xie, Q., Wu, D., Wang, X., Li, Y., Fang, F., Wang, Z., Ma, Y., Su, M., Peng, S., Liu, H., Wang, K., & Sun, X. W. (2019). Branched capping ligands improve the stability of cesium lead halide (CsPbBr3) perovskite quantum dots. *Journal of Materials Chemistry C, 7*(36), 11251-11257. https://doi.org/10.1039/c9tc03377g

Xiong, X., Wei, C., Xie, L., Chen, M., Tang, P., Shen, W., Deng, Z., Li, X., Duan, Y., Su, W., Zeng, H., & Cui, Z. (2019). Realizing 17.0% external quantum efficiency in red quantum dot light-emitting diodes by pursuing the ideal inkjet-printed film and interface. *Organic Electronics, 73,* 247-254. https://doi.org/10.1016/j.orgel.2019.06.016

Yang, P., Zhang, L., Kang, D. J., Strahl, R., & Kraus, T. (2020). High-Resolution Inkjet Printing of Quantum Dot Light-Emitting Microdiode Arrays. *Advanced Optical Materials, 8*(1), 1-7. https://doi.org/10.1002/adom.201901429

Yang, X., Zhang, Z. H., Ding, T., Wang, N., Chen, G., Dang, C., Demir, H. V., & Sun, X. W. (2018). High-efficiency all-inorganic full-colour quantum dot light-emitting diodes. *Nano Energy, 46,* 229-233. https://doi.org/10.1016/j.nanoen.2018.02.002

Yang, Y., Qin, H., Jiang, M., Lin, L., Fu, T., Dai, X., Zhang, Z., Niu, Y., Cao, H., Jin, Y., Zhao, F., & Peng, X. (2016). Entropic Ligands for Nanocrystals: From Unexpected Solution Properties to Outstanding Processability. *Nano Letters, 16*(4), 2133-2138. https://doi.org/10.1021/acs.nanolett.6b00730

Yi, Y. Q. Q., & Su, W. (2023). Cross-linking strategies for hole transport/emissive layers in quantum-dot light-emitting diodes. *Materials*

Chemistry Frontiers, 7(23), 6130-6140. https://doi.org/10.1039/d3qm00831b

Zhan, S., Suh, Y. H., Fan, X. B., Yang, J., Ni, L., Kim, Y., Jo, J. W., Choi, H. W., Jung, S. M., Shin, D. W., Lee, S., & Kim, J. M. (2022). Inkjet-printed multi-color arrays based on eco-friendly quantum dot light emitting diodes with tailored hole transport layer. *Journal of the Society for*

Information Display, 30(10), 748-757. https://doi.org/10.1002/jsid.1133

Zhu, T., Shanmugasundaram, K., Price, S. C., Ruzyllo, J., Zhang, F., Xu, J., Mohney, S. E., Zhang, Q., & Wang, A. Y. (2008). Mist fabrication of light emitting diodes with colloidal nano-crystal quantum dots. *Applied Physics Letters, 92*(2), 10-13. https://doi.org/10.1063/1.2834734

❧❦